Green's function calculations of the hyperfine interaction for impurities in metals and for metallic interfaces

P.H. Dederichs, P. Lang, K. Willenborg, R. Zeller

Institut für Festkörperforschung, Forschungszentrum Jülich, Postfach 1913, D-5170 Jülich, Germany

N. Papanikolaou and N. Stefanou

Solid State Section, University of Athens, Panepistimioupolis, New Buildings, GR-157 84, Athens, Greece

We present local density functional calculations for magnetic impurities and magnetic monolayers in non-magnetic metals. The calculations employ a multiple scattering (KKR) Green's function method for impurities in the bulk and for ideal surfaces and interfaces. In particular we discuss the moment formation of 3d and 4d impurities in alkali and noble metals. Special emphasis is put on an accurate calculation of the host polarization around 3d impurities in Cu and Pd. While the calculated impurity hyperfine fields in Cu contain rather large errors due to the local density approximation, the induced fields of the Cu atoms agree very well with experiments. We also present similar calculations for magnetic monolayers and the corresponding induced host polarization in Cu and Pd.

1. Introduction

The aim of this article is to review recent electronic structure calculations for magnetic impurities and magnetic monolayers in non-magnetic metals. All calculations are based on the local density approximation of density functional theory [1] and apply Green's function methods to solve the Kohn–Sham equation for a point defect [2] and for a planar defect [3], both embedded in an otherwise ideal crystal. A short description of these methods is given in section 2.

The first system which we want to discuss is magnetic impurities in alkali metals, a field which has been pioneered by the experimental work of Riegel and coworkers [4–7]. In addition to the Green's function calculations we apply the simple jellium model to discuss the formation of local moments in these exotic hosts. In the heavier alkali metals practically all transition-metal impurities of the 3d and 4d series should be magnetic, with very large local moments. In addition to the d moment also a sizeable s moment can develop which strongly influences the hyper-

fine field of the impurity. Due to the large size differences between the impurity and the host atoms and due to the "ionic" impurity configurations observed a satisfactory theoretical description is still missing. As an addenda to these calculations we discuss the simpler case of 3d impurities in the noble metals. Here we point to some problems of the local density approximation with respect to the hyperfine fields of the impurities.

The following section is devoted to the polarization being induced by the impurities into the host matrix. We present accurate calculations by including several hundreds of impurity atoms into the self-consistency process. For 3d impurities in Cu we find the expected Friedel-like, i.e. oscillatory, behavior of the host polarization, however, with large anisotropies resulting from the anisotropy of the Fermi surface. The calculated hyperfine fields are in very good agreement with Knight-shift data obtained by the Slichter group (see references given in ref. [8]). For 3d impurities in Pd the exchange enhancement of the host is very important leading to an, essentially exponential, decrease of the host polarization.

In section 5 we discuss the host polarization around magnetic (100) monolayers of Fe and Co atoms embedded into Cu and Pd hosts. By calculating the host polarization in Cu up to twelve layers away from the impurity layer, we find an oscillatory behavior with an amplitude decreasing as $1/D^2$, where D is the distance from the impurity layer. In line with Fermi-surface arguments, more than one oscillation period seems to exist. In contrast to this the polarization in Pd decreases monotonously with no indication of oscillations.

2. Method of calculation

The calculations are based on density functional theory in the local density approximation (LDA) [1]. The effective one-particle equations of this theory are solved by a Green's function approach. The Green's function of the system with defect, $G(\boldsymbol{r}, \boldsymbol{r}'; E)$, is related to the reference Green's function of the ideal crystal, $\mathring{G}(\boldsymbol{r}, \boldsymbol{r}'; E)$, by a Dyson equation

$$G(\boldsymbol{r}, \boldsymbol{r}'; E) = \mathring{G}(\boldsymbol{r}, \boldsymbol{r}'; E) + \int \mathrm{d}\boldsymbol{r}'' \mathring{G}(\boldsymbol{r}, \boldsymbol{r}''; E) \Delta V_{\mathrm{eff}}(\boldsymbol{r}'') G(\boldsymbol{r}'', \boldsymbol{r}'; E) \,. \tag{1}$$

Here $\Delta V_{\mathrm{eff}}(\boldsymbol{r})$ is the change of the effective potential V_{eff} of the host induced by the defect. The key to the solution (1) is that the potential perturbation is spatially localized close to the defect. For an impurity, typically, we take the impurity potential and several shells of perturbed host potentials into account. We will sketch now this method for the case of muffin-tin potentials centered at positions $\boldsymbol{R}^n$. In this case, the Green's function $G(\boldsymbol{r} + \boldsymbol{R}^n, \boldsymbol{r}' + \boldsymbol{R}^n; E)$ is expanded in each cell into the eigensolutions of these spherically symmetric local potentials:

$$G(\boldsymbol{r}+\boldsymbol{R}^n, \boldsymbol{r}'+\boldsymbol{R}^{n'}; E) = \sqrt{E}\,\delta_{nn'} \sum_L Y_L(\boldsymbol{r}) H_l^n(r_>; E) R_l^n(r_<; E) Y_L(\boldsymbol{r}') + \sum_{L,L'} Y_L(\boldsymbol{r}) R_l^n(r; E) G_{LL'}^{nn'}(E) R_{l'}^{n'}(r'; E) Y_{L'}(\boldsymbol{r}') . \quad (2)$$

Here the vectors $\boldsymbol{r}$ and $\boldsymbol{r}'$ are restricted to the Wigner–Seitz cell and $r_>$ ($r_<$) denotes the larger (smaller) value of $r = |\boldsymbol{r}|$ and $r' = |\boldsymbol{r}'|$. The subscript $L = (l, m)$ denotes angular momentum numbers and $Y_L(\boldsymbol{r})$ are real spherical harmonics. $R_l^n(r, E)$ and $H_l^n(r, E)$ are the regular and irregular solutions of the radial Schrödinger equation for the nth muffin-tin potential.

All information about the multiple scattering is contained in the structural Green's function matrix $G_{LL'}^{nn'}(E)$. By inserting (2) for the defect Green's function G and the analogous equation for the ideal Green's function $\mathring{G}$ into the Dyson equation (1), this integral equation is transformed into an algebraic Dyson equation for the structural matrices $G_{LL'}^{nn'}(E)$.

$$G_{LL'}^{nn'}(E) = \mathring{G}_{LL'}^{nn'}(E) + \sum_{n''L''} \mathring{G}_{LL''}^{nn''}(E) \Delta t_{l''}^{n''}(E) G_{L''L'}^{n''n'}(E) . \quad (3)$$

The summation goes over all sites n'' and angular momenta L'' for which the perturbation $\Delta t_l^n(E) = t_l^n(E) - \mathring{t}_l^n(E)$ of the t-matrices of the host is significant. Typically we take several shells of perturbed atoms and all angular momenta up to $l = 3$ into account.

The charge density can be directly calculated from the imaginary part of the Green's function,

$$n(\boldsymbol{r}) = -\frac{2}{\pi} \int^{E_F} \mathrm{d}E\, \mathrm{Im}\, G(\boldsymbol{r}, \boldsymbol{r}; E) . \quad (4)$$

The extension to spin-polarized problems is straightforward. More details about the KKR–Green's function method and the calculations can be found in ref. [2].

The above formalism can also be extended to planar defects, e.g. a surface or a monolayer of impurities [3]. In the latter case we replace a whole monolayer of host atoms by impurities. The perturbed potential $\Delta V_{\mathrm{eff}}(\boldsymbol{r})$ is then localized in the direction perpendicular to the plane, say with perturbed potentials on the impurity monolayer and a few adjacent host layers. The infinite extent of the perturbation in the plane can be taken into account by exploiting the two-dimensional planar periodicity and performing a two-dimensional Fourier transform. The resulting Green's function,

$$G_{LL'}^{jj'}(\boldsymbol{k}_\parallel, E) = \sum_m \mathrm{e}^{\mathrm{i}\boldsymbol{k}_\parallel \boldsymbol{R}^m} G_{LL'}^{nn'}(E) , \quad (5)$$

is indexed by layer indices jj' and angular momenta LL', with $\boldsymbol{k}_\parallel$, the k-vector of the two-dimensional Fourier transform, as an additional parameter. Here the three-dimensional lattice index n is split up into a layer index j and a two-dimen-

sional index m covering the sites within a layer. The Fourier transform of (3) then leads to an equation

$$G^{jj'}_{LL'}(\boldsymbol{k}_\parallel, E) = \mathring{G}^{jj'}_{LL'}(\boldsymbol{k}_\parallel, E) + \sum_{j''L''} \mathring{G}^{jj''}_{LL''}(\boldsymbol{k}_\parallel, E)\Delta t^{j''}_{l''}(E) G^{j''j'}_{L''L'}(\boldsymbol{k}_\parallel, E)\,, \tag{6}$$

which has the form of the Dyson equation of a linear chain with a localized perturbation.

In order to describe a surface we remove a few monolayers, typically 3–5, from the ideal crystal. The resulting two half-crystals are practically decoupled, since the valence electrons cannot penetrate the vacuum barrier created by the removal of the host layers.

In order to obtain the charge density $n(\boldsymbol{r})$ the energy integration in (4) is performed along a contour in the complex energy plane [2] which starts below the valence band minimum at the real axis, proceeds into the complex energy plane and comes back to the real axis at the Fermi energy. For the impurity calculations a mesh of about 30 to 60 energy points is used, which becomes increasingly finer close to E_F. For the monolayer calculations, we introduce a Fermi distribution function with a temperature of $kT = 3$ m Ry in order to smoothen the occupation cut-off at the Fermi energy. Due to the poles of the Fermi distribution function for complex energies, this leads to an equidistant mesh of complex energy points close to E_F. The additional $\boldsymbol{k}_\parallel$ integration, required to obtain the charge density, is performed by the special point method. In order to obtain accurate Friedel oscillations at large distances, a large number of $\boldsymbol{k}_\parallel$ points is required. For the (100) geometry we use 465 points in the irreducible part of the planar Brillouin zone.

3. Magnetic impurities in monovalent metals

3.1. 3d AND 4d IMPURITIES IN ALKALI METALS

In recent years Riegel and co-workers [4–7] have performed extensive studies of the behavior of magnetic impurities in simple metals, especially of 3d and 4d impurities introduced into alkali metal hosts by ion implantation. These experiments have motivated the present study in which we have calculated the magnetic properties of transition metal impurities in the alkalis both by a jellium model and by the KKR Green's function method [9].

Due to the large elementary volumes of the alkali metals, transition metal impurities experience a strong tendency for moment formation in these hosts, being larger than in any other metallic system. This is nicely demonstrated in jellium calculations for the non-spin polarized states. In these calculations the host is simulated by a jellium of constant density $\bar{\rho}$ being determined by the reciprocal of the host volume. The noble metals are also considered as monovalent. In order to describe the impurity, one cuts a spherical hole, i.e. a vacancy, into the jellium, into

which the impurity potential is inserted. Table 1 lists the widths of the virtual bound states of two typical impurities from the middle of the 3d and 4d row, i.e. Mn and Tc, being isoelectronic. Between the most dense Cu host and the most diluted Cs host at the other end the widths of the virtual bound states dramatically decrease by about a factor 20. Thus the host density is the most important parameter compared to which the difference between the 3d and 4d impurities is of minor importance. The results clearly show that in the heavier alkali metals both the 3d and the 4d impurities are quite close to the atomic limit.

The condition for the occurrence of a local impurity moment according to Blandin [10] is given by $In_{\mathrm{loc}}(E_{\mathrm{F}}) > 1$, where I is the exchange integral and $n_{\mathrm{loc}}(E_{\mathrm{F}})$ the paramagnetic local density of states of the impurity at the Fermi energy. Fig. 1 shows the critical jellium densities $\bar{\rho}_{\mathrm{c}}$ for the formation of local impurity moments. For host densities $\bar{\rho} < \bar{\rho}_{\mathrm{c}}$ the impurities are magnetic. Both curves for the 3d and 4d impurities exhibit a similar parabolic behavior with a maximum in the middle of the series.

Physically, the most important difference between 4d and 3d impurities is the somewhat larger spatial extent of the 4d wave function, which leads to a stronger hybridization with the host and to a slightly smaller exchange integral. Both facts are unfavorable for spin-polarization and represent the basic reasons why 4d metals and the corresponding alloys are normally non-magnetic. As a further consequence, 4d impurities become magnetic only at more dilute jellium densities than their 3d counterparts, as is illustrated in fig. 1. Within a given series the condition for magnetism is most likely to be met when the virtual bound state is close to the Fermi energy, since the exchange integral does not vary strongly within the series. Therefore, impurities with a half-filled d shell, i.e. Cr, Mn or Mo, Tc, show the strongest tendency to spin-polarization and thus become magnetic in a wider range of jellium densities and have the largest local moments in a given simple-metal host. This is confirmed by our calculations. As can be seen from fig. 1, the $\bar{\rho}_{\mathrm{c}}$ curve for the 4d series is slightly shifted to lower valencies as compared to the corresponding 3d curve. This is basically caused by the shift of the atomic 5s level of the 4d atoms to higher energies, leading to smaller s counts and larger d counts in the 4d series as compared to the 3d one. This explains why the maximum of the $\bar{\rho}_{\mathrm{c}}$ curve occurs in the 4d series at Nb and Mo as compared to Cr and Mn in the 3d ser-

Table 1
Half-width Δ of virtual bound states of Mn and Tc impurities in monovalent metal hosts, as obtained in non-spin-polarized jellium calculations (units: eV).

Impurity	Host						
	Cu	Ag	Li	Na	K	Rb	Cs
Mn	0.90	0.53	0.47	0.21	0.08	0.06	0.04
Tc	1.50	0.92	0.77	0.35	0.14	0.10	0.07

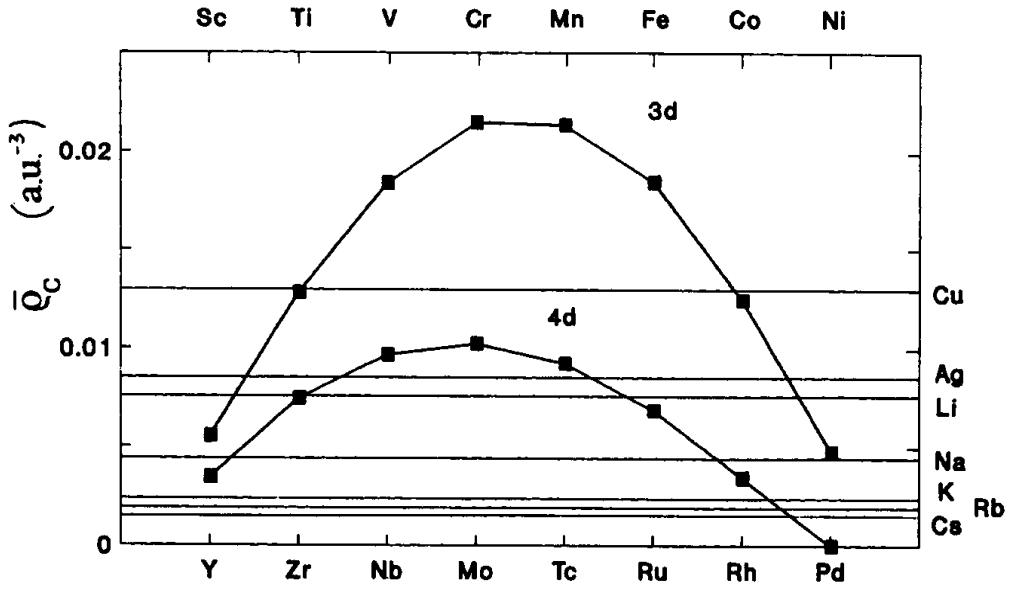

Fig. 1. Critical densities of jellium host, $\bar{\rho}_c$, below which the impurity becomes magnetic. The parallel lines to the abscissa correspond to the jellium densities of (from up to down): Cu, Ag, Li, Na, K, Rb, Cs.

ies and why Pd does not become magnetic even in K, Rb or Cs (even a free Pd atom has a zero spin-moment), where Ni is strongly magnetic (see below).

From the behavior of the $\bar{\rho}_c$ curves for the 3d and 4d impurities one might guess that also impurities of the 5d series should become magnetic in these exotic hosts. Thus we believe that the substitutional 5d impurities from the middle of the series are magnetic in the heavier alkali hosts. This is also indicated by the halfwidths of 3d and 4d impurities listed in table 1, which suggests similar small values also for 5d impurities.

The moments of the transition metal impurities in the heavier alkali metals are quite large, with the d moments being practically saturated. A detailed account is given in ref. [9]. Fig. 2 shows the local moments of Cr, Mn and Mo, Tc impurities in Jellium as a function of the jellium density $\bar{\rho}$, normalised by the critical density $\bar{\rho}_c$. The special symbols show the results of more realistic KKR Green's function calculations. The good agreement indicates that the jellium model gives a realistic description of the alkali metals. In the vicinity of the transition from the spin-polarized to the non-spin-polarized impurity state, the local moment varies as

$$M_{\mathrm{loc}} \cong M_0(1 - \rho/\rho_c)^{1/2} \tag{7}$$

as one expects for a second-order transition. This dependence is given by the dashed line in fig. 2 and also applies for jellium densities further away from the transition.

The moments of Cr and Mo even exceed the limit of 5 μ_B, the maximal d moment possible. The reason for this is that under such diluted conditions the transition

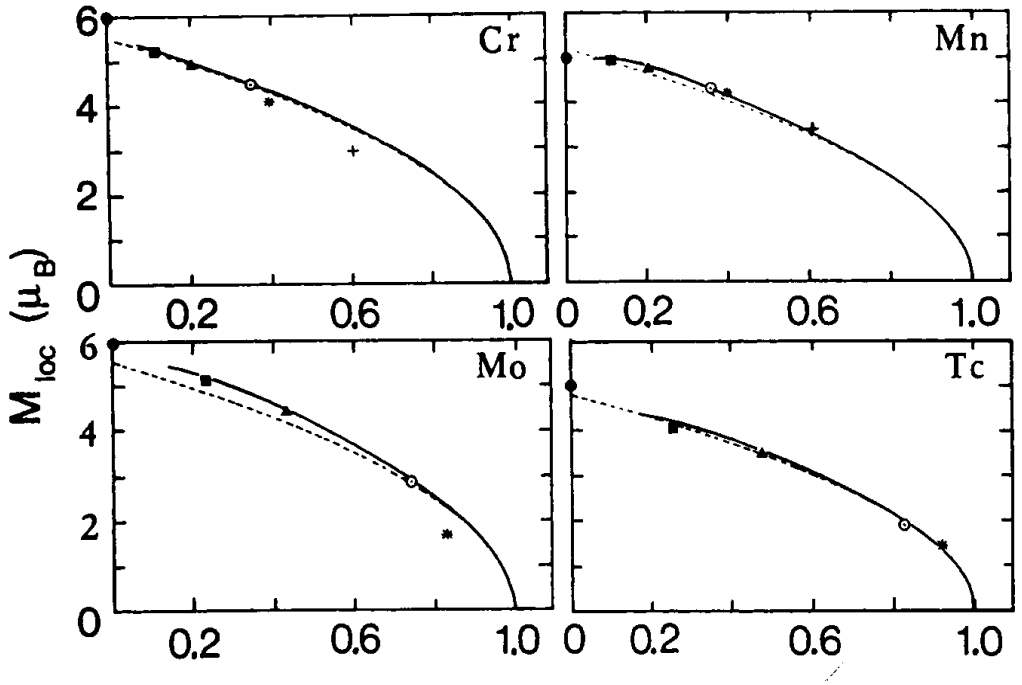

Fig. 2. Local moments of 3d impurities in jellium (full curve). The dashed curve refers to the result of the interpolation formula. The symbols +, *, ⊙, △, □ show the KKR results in Cu, Ag, Li, Na and K hosts respectively. The dots (for $\bar{\rho} = 0$) represent the atomic spin-moments.

metal impurities also develop a sizeable s moment, as it naturally occurs for the free atoms. This is illustrated in table 2, where the s, p and d contributions to the moment of a Cr impurity in various hosts are given. In the noble metals the non-d components of the moments are very small, typically 0.01 μ_B. However already in Na sizeable s and p moments develop, e.g. about 0.18 and 0.12 μ_B for the Cr impurity. Due to the strong decrease of the Fermi energy of the host, the s moment of Cr then further increases to 0.40 μ_B in Cs, whereas the p moment slowly increases to 0.16 μ_B in K, and then decreases to 0.14 in Rb and 0.11 μ_B in Cs. This behavior is

Table 2
Angular momentum decomposition of the local moment of a Cr impurity in monovalent metal hosts (units: μ_B) according to KKR and jellium (for Rb and Cs) calculations.

	Cu	Ag	Li	Na	K	Rb	Cs
M_s	0.03	0.06	0.09	0.18	0.26	0.36	0.40
M_p	0.03	0.06	0.09	0.12	0.16	0.14	0.11
M_d	2.93	3.97	4.29	4.60	4.78	4.85	4.89
M_{tot}	2.99	4.09	4.47	4.90	5.20	5.35	5.40
H_{core}	−289	−397	−427	−450	−460	–	–
H_{val}	173	299	412	569	696	–	–
H_{tot}	−116	−98	−16	119	236	–	–

to be expected since in the atomic limit (configuration $3d^5 4s^1$) the p moment vanishes whereas the s moment is 1 μ_B. Similar sp moments are also calculated for 4d impurities, e.g. for a Mo impurity an s moment of 0.37 μ_B is obtained in Rb and 0.41 μ_B in Cs. Thus for the systems considered we have a twofold transition to the atomic limit, the one for the d electrons which is essentially completed already for Na or K, and the one for the s and p levels, which we just begin to notice at Cs. This is of course a direct consequence of the much larger spatial extent of the s and p wavefunctions.

The s moments are very important for the hyperfine fields of the impurities. The calculated hyperfine fields for a Cr impurity are also listed in table 2, separately for the core- and valence contributions together with the total fields. The core polarization arizing from the intra-atomic s–d exchange varies linearly, but oppositely in sign, with the local d moment, which is also confirmed in our calculations. Unfortunately this contribution is underestimated in local density functional theory by as much as about 30% (see below). However, here the important point is that the formation of an s moment leads to a strong positive contribution which in the heavier alkali metals cancels the negative core contribution so that the total hyperfine field becomes strongly positive. Due to the underestimation of the core field this might not happen in reality so that relatively small negative or slightly positive values could be expected in cases such as Cr and Mo where no orbital moment exists.

The present description of transition-metal impurities in the alkali metals is very much simplified. In fact for two reasons we believe that these systems are much more difficult than, e.g., 3d impurities in Cu. Firstly there are the large size differences due to the unusually large volumes of the alkali metals. As discussed by Riegel and coworkers [7] this might lead to unusually large lattice relaxations of the neighboring atoms. One might also think of off-center or interstitial positions rather than substitutional positions as assumed here. In all these cases we expect the s moment to be strongly reduced by the increasing hybridization with the host, while the d moment should be rather insensitive. Thus the hyperfine field could be a sensitive probe for such environmental changes. Clearly reliable ab initio calculations including lattice relaxations and non-substitutional positions are urgently needed. The second complication arises from the orbital moments of these impurities. While in the noble and transition metals the orbital moments are quenched to a high degree, in the simple metals usually the full atomic orbital moments are observed as requested by Hund's second rule. Unfortunately, density functional theory in the local density approximation is not able to describe such orbital polarizations, basically because it is not free of spurious self-interactions. More refined treatments such as self-interaction corrections are necessary. In a recent paper we have examined such effects in the LDA + U approximation [11]. Except for filled or half filled bands we find strong polarization effects and highly ionic configurations, even indications of valence fluctuations. Thus more theoretical work is necessary to understand these interesting systems.

3.2. MOMENTS AND HYPERFINE FIELDS OF 3d IMPURITIES IN Cu AND Ag

Traditionally the hyperfine field of an atom in a solid has been thought to consist of two contributions, a local and a transferred contribution. While these parts are difficult to distinguish in actual calculations, their different physical origin is reasonably clear. The local contribution is due to the intra-atomic exchange interaction between the strongly polarized d electrons and the s electrons, thus leading to an s polarization at the nucleus. The transferred contributions arise from the hybridization of the local orbitals with the spin-polarized orbitals of the neighboring atoms, or, in the language of scattering theory, from the scattering of the wave function at the spin dependent potentials of the neighboring sites. As argued by Blugel et al. [12] the local contributions cannot be calculated well in density functional theory, since the very non-local intra-atomic sd exchange is only crudely described in the local density approximation. The transferred fields, on the other hand, are very well given in the local density approximation, since they are determined by the interatomic hybridization.

Whereas in normal alloys usually both contributions to the hyperfine field are important and only the sum can be measured, magnetic impurities in noble metals are nice model systems where only the local contribution is important, since the moments of the neighboring host atoms are two orders of magnitude smaller than the impurity moments. For the same reason the host hyperfine fields have practically only transferred contributions, arising from the scattering of the host states at the spin-split impurity potentials. Therefore we expect, and this is demonstrated by the following results, that the calculated impurity hyperfine fields contain relatively large errors. On the other hand the induced hyperfine fields of the host atoms should be well described by the local density approximation, which is confirmed by the results presented in the next section.

Table 3 gives the results of non-relativistic calculations for local moments and hyperfine fields of 3d impurities in Cu and Ag. Given are the local s moments M_s, the total moments M_t, the hyperfine fields due to the core (H_{core}) and valence electrons (H_{val}) as well as the total hyperfine fields H_{tot} and some few experimental fields [13]. Whereas the core field is very well given by the d moment, the s moment determines essentially the valence field, with the ratio H_{val}/M_s being more or less constant in each series, but appreciably smaller in the Ag host. The latter fact has to do with the larger volume of Ag (see also fig. 1). By comparing with the experimental values, we see that the calculated hyperfine field for Mn in Cu is about a factor 2 too small, whereas in Ag this is even a factor 3.7. Note that the calculations refer to a non-relativistic treatment; a scalar relativistic treatment should lead to a small enhancement of the values by about 7.5% for Mn. In addition there is a unknown contribution from the orbital hyperfine field. However, both contributions are by far not large enough to explain the discrepancies. Assuming that the valence field is reasonably well given in LDA, the calculated core hyperfine field would have to

Table 3
Moments and hyperfine fields of 3d impurities in Cu and Ag. Given are the s moments M_s, the total moment M_t, the core and valence contributions to the hyperfine fields as well as the total hyperfine field together with experimental values [13].

	V	Cr	Mn	Fe	Co
host Cu					
M_s	0.009	0.028	0.030	0.020	0.006
M_t	0.90	2.94	3.37	2.49	0.89
H_{core}	−86.4	−288.7	−337.0	−252.0	−92.7
H_{val}	53.7	172.7	194.6	135.0	44.5
H_{tot}	−32.7	−115.9	−143.0	−117.0	−48.2
H_{exp}		−153±10	−280±10	−151	
			−295±20		
host Ag					
M_s	0.049	0.067	0.068	0.043	0.020
M_t	2.91	4.09	4.17	3.01	1.60
H_{core}	−274.4	−397.4	−416.6	−305.7	−167.1
H_{val}	208.2	299.1	328.7	220.5	104.5
H_{tot}	−66.3	−98.3	−88.0	−85.1	−62.7
H_{exp}			−328±10		

be enlarged by as much as 50% in order get reasonable values for the hyperfine fields of Mn.

4. Magnetization oscillations around 3d impurities in Cu and Pd

The magnetization disturbance induced into the host metal is another important finger print of a magnetic impurity. Due to the efficient short-range-screening in metals the charge and magnetization oscillations in the host are usually very small effects and therefore difficult to calculate. Typically a Cu atom being a nearest neighbor of a 3d impurity carries an induced moment of about $10^{-2}\,\mu_B$, which rapidly decreases with distance. Despite of this, very nice experimental information about the magnetization oscillations in Cu exists due to the measurements of Knight-shift satellites by the Slichter group [8]. A detailed comparison between the calculations of the hyperfine fields for the first six shells of Cu atoms and the measured Knight-shift satellites has been published [8]. Due to the recent strong interest in interlayer coupling induced by RKKY interactions and the absence of other reliable ab-initio results we have extended these calculations by including the first 12 shells of Cu atoms, i.e. 225 atoms in total, into the self-consistency process. We report also about similar calculations for 3d impurities in Pd, where in a tour de force calculation up to 40 shells (1061 atoms) have been considered [14].

The relation between the measured Knight-shift satellites and the calculated hyperfine fields is non-trivial; for details we refer to ref. [8]. The temperature

dependence of the Knight shifts is basically determined by the impurity susceptibility and is the same for all satellites where as the shell dependence is given by the hyperfine fields. Fig. 3 shows the calculated hyperfine fields for the Cu atoms of the first 12 shells, separately for the three cases of Cr, Mn and Fe impurities. Since the amplitude of the Friedel oscillations should vary with distance R as $1/R^3$, we have plotted the product of the hyperfine field H_n with the third power of the distance R_n. Therefore in a free electron model one expects a pure oscillation $\sim \cos(2k_F R+\delta)$, where k_F is the Fermi wavevector and δ the impurity phase shift. Indeed the dashed curves in fig. 3, representing the results of selfconsistent impurity-in-jellium calculations, resemble such a behavior. In these calculations the jellium results have been adjusted to the KKR results for the first nearest neighbors. This is necessary since in the jellium approach the effect of the core oscillations cannot be included.

The more realistic KKR Green's function calculations, which include all band structure effects, show important deviations from the simple $\cos 2k_F R$ behavior. These are connected with the anisotropy of the band structure and the Fermi surface leading to an anisotropic disturbance of the charge and magnetization densities, which depend not only on the distance $R_n = |\boldsymbol{R}_n|$, but also on the direction $\hat{\boldsymbol{R}}_n$. Therefore a plot of the hyperfine fields H_n versus the distance $|\boldsymbol{R}_n|$ shows some irregular behavior. The direction dependence becomes especially clear when we consider the two shells (411) and (330), having the same distance $|\boldsymbol{R}_n|$, but hyperfine fields differing by a factor of eight.

The behavior of the oscillations in real space is intimately connected with the detailed properties of the Fermi surface, as has been demonstrated by Roth et al. [15]. Asymptotically one obtains for a given direction R_n only contributions from those points $\boldsymbol{k}$ on the Fermi surface, the group velocity $\boldsymbol{v}_k$ of which points parallel or antiparallel to $\hat{\boldsymbol{R}}_n$. The period of oscillation is determined by the caliper of the Fermi surface between such points with opposite group velocity, the amplitude by the curvature of the Fermi surface at these points. In our calculations we find especially large hyperfine fields for the shells (110), (220), (330) which can be traced back to the flattening of the Fermi surface in (110) direction, leading to a small curvature and a large amplitude of the hyperfine fields. Also the appearance of a superperiod in this direction can be seen.

The calculations show that a non-selfconsistent treatment of the host gives already the correct trends for the magnetization disturbance. A self-consistent calculation of the host polarization changes the magnetization distribution only by 10–20%, while the charge distribution is somewhat more affected. Basically this is due to the fact that the spin susceptibility $\chi = S\chi_0$ of the noble metals is essentially given by the Pauli susceptibility χ_0, since the Stoner enhancement factor $S \cong 1.12$ [16]. Note that the direct relation of the oscillations to the Fermi surface properties is only valid if the selfconsistent enhancement of the polarization can be neglected, i.e. if $S \approx 1$.

In a previous publication [8] we have made a detailed comparison with the

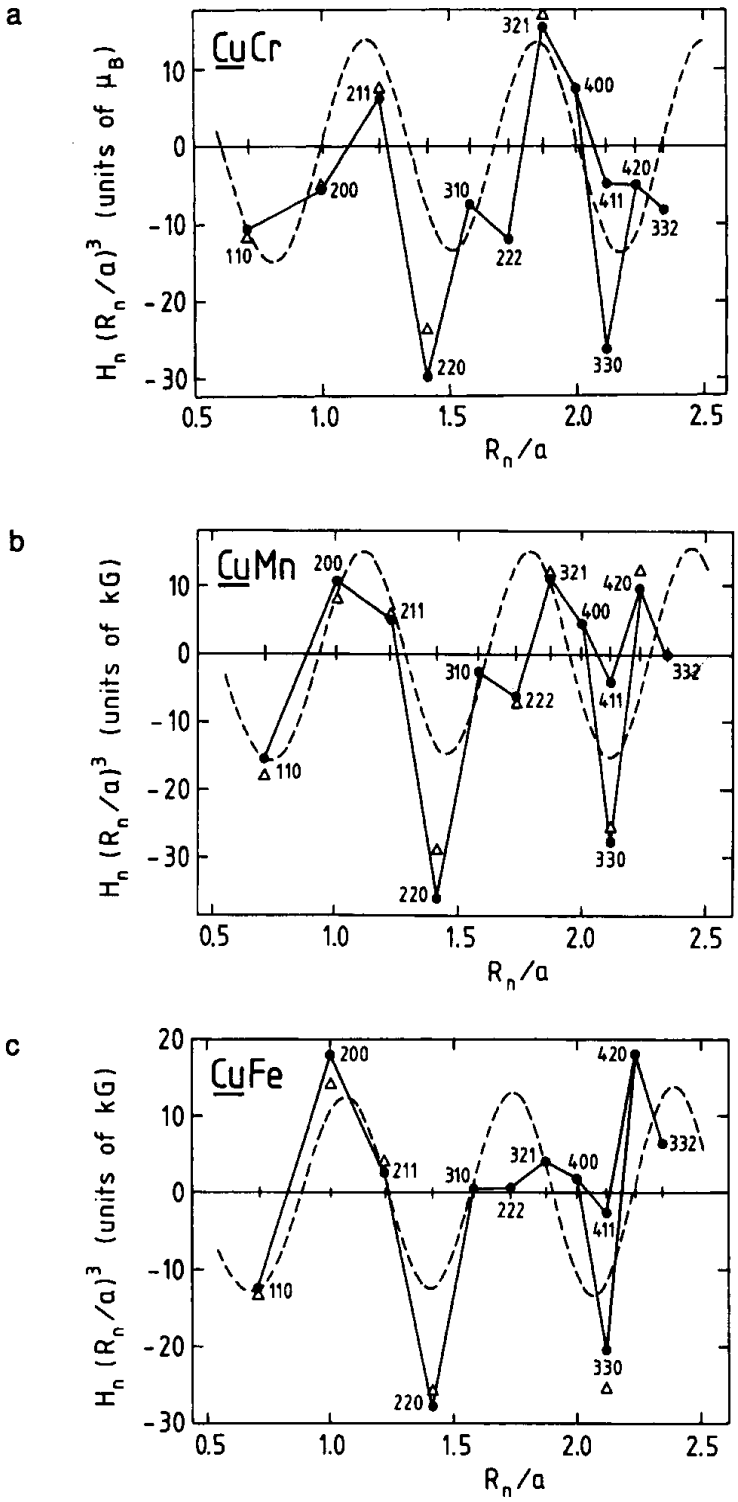

Fig. 3. Hyperfine fields H_n of Cu atoms in the nth shell around Cr impurities (a), Mn (b) and Fe impurities in Cu. (c) Plotted are the hyperfine fields multiplied by $(R_n/a)^3$, where R_n is the distance of the nth shell and a the lattice constant.

experimental results of the Slichter group which was, however, restricted to the hyperfine fields of the first four shells. Here we will shortly comment on the outer shells. The experimental value for the hyperfine fields are indicated by triangles in fig. 4, with the assignment as made in the present paper. For **CuCr** peak N can be ascribed to the seventh shell (321), with the assignment being supported both by the relatively large value of field as well as the large intensity corresponding to a shell of 48 atoms. The assignment of peak P (8th shell?) and peak C (5th, 6th or 9th shell or a combination of these) is not clear. In addition we believe that the field of the second shell has actually been observed, but wrongly interpreted. For **CuMn** we obtain good agreement with all observed satellites. Based on the value of the field and the intensity of the satellite we assign peak C to the 9th shell (330) and on the same grounds peak P to the 7th shell (321). Moreover from the values of the fields we assign peak D to the 6th shell and peak Q to the 11th one. In the case of **CuFe** we can relate peak C which was erroneously assigned to the 4th shell (220), to the 9th shell (330). Since both shells have the same symmetry, they cannot be distinguished in the experiments.

While the present discussion is restricted to the isotropic Fermi contact interaction, we have recently also studied the anisotropic dipolar interaction [17] leading to an additional splitting of the satellites. Also these results are in good, but not perfect agreement with the experiment, pointing out the importance of the dipolar interaction as the most important source of anisotropic hyperfine interaction.

An extreme case, where the self-consistent evaluation of the magnetization is very important, is represented by 3d impurities in Pd. The pure host Pd has a Stoner

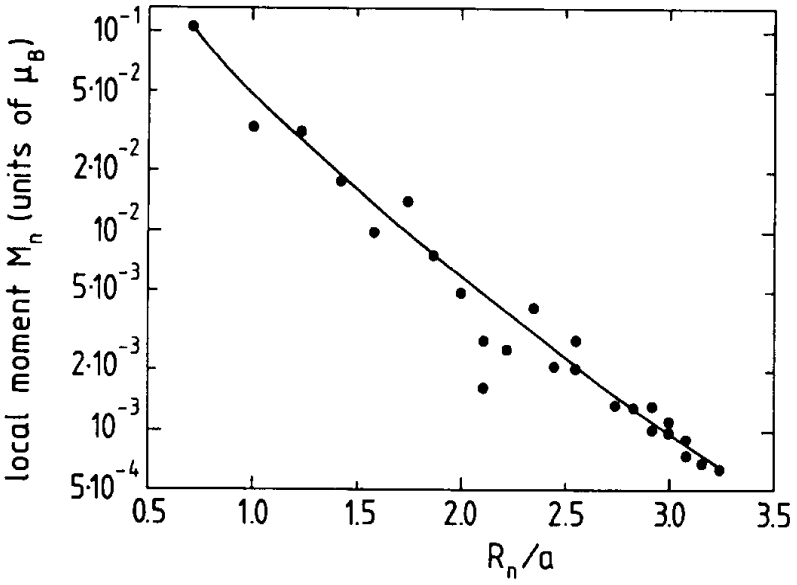

Fig. 4. Host polarization around Fe impurities in Pd. The semilogarithmic plot shows the local moments M_n of Pd atoms in the first 25 shells around the impurity. The full line represents the least square fit to the calculated values.

enhancement factor $S \approx 8$ and can therefore be considered as nearly ferromagnetic. Consequently, magnetic 3d impurities induce large host polarizations. The total moment per impurity, consisting of the impurity moment and the moment of the polarization cloud, can be as large as $10\,\mu_B$ and is referred to as giant moment. An interesting question concerns the spatial extent and variation of the polarization cloud. From neutron scattering measurements the clouds are generally believed to be rather extended, containing up to 200 host atoms. Model calculations based on the behavior of the enhancement factor $S(q)$ for small q-values, predict an exponential variation of the polarization: $m(R) \sim e^{-\kappa R}$. In contrast to this monotonous variation with R one might expect a oscillatory behavior for larger distances.

Recently one of us has performed large scale calculations to examine the form of the polarization cloud [14]. These are extensions of previous calculations by our group [18], now including up to 40 shells, i.e. in total 1061 atoms, into the self-consistency process. The results for Fe impurities in Pd are shown in fig. 5, where in a semilogarithmic representation the induced Pd moments for the first 25 shells are plotted versus the distance R from the impurity. The moments range from $10^{-1}\,\mu_B$ for the first shell to values of $10^{-3}\,\mu_B$ and smaller for shell numbers larger than 20. The full line refers to the function

$$M_n = \frac{0.199\, e^{-1.41 R_n/a}}{R_n/a}\ (\mu_B)$$

which has been obtained by a least square fit to the calculated values. While this curve resembles the overall behavior reasonably well, the individual points scatter

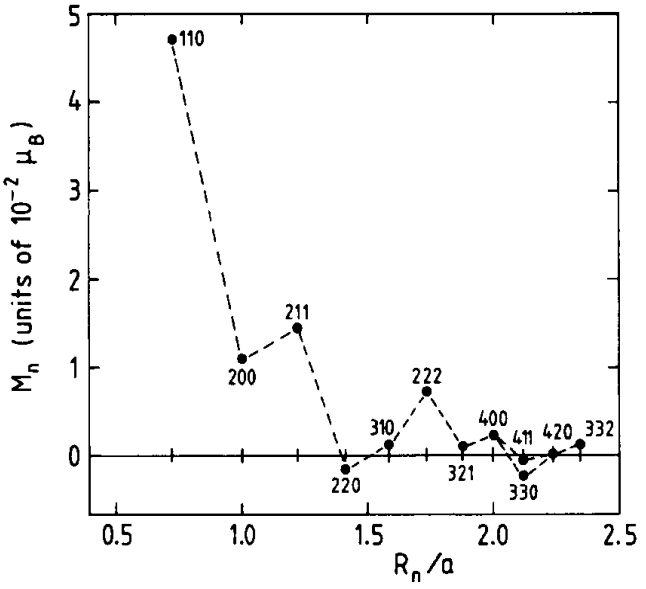

Fig. 5. Host moments M_n around Mn impurities in Pd (in μ_B).

quite a bit, indicating an important anisotropy of the moment distribution. It is noteworthy, however, that even up to 40 shells the calculations for Fe, Co and Ni impurities do not yield negative moments or any other sign of oscillations. For Mn impurities, on the other hand, some negative moments are obtained, e.g. for the fourth shell (220) and the ninth and tenth shells as is shown in fig. 5. For Cr impurities, the polarization cloud couples antiparallel to the impurity moment. Thus in total, the magnetization distribution in Pd is dominated by the strong exchange enhancement. No indications of oscillations are found, with the exception of Mn impurities where for certain shells small negative moments are found.

5. Magnetic monolayers and host polarization in Cu and Pd

Due to the advancement of molecular beam epitaxy, truly two-dimensional magnetic behavior can nowadays be studied in the form of thin films or ideally in the form of magnetic monolayers. Theoretical predictions of magnetic overlayers or interlayers [19,20] with greatly enhanced moments have strongly motivated these studies. Here we present some new calculations based on the KKR Green's function method for 3d monolayers on Cu(001) and for (001) monolayers sandwiched in bulk Cu. The main emphasis will be on the difference between the local moments for the two different geometric environments and on the oscillatory behavior of the induced host polarization. Similar results are also reported for an Fe monolayer in Pd.

Table 4 shows the calculated local moments of (100) monolayers of Fe, Co and Ni grown epitaxially on the Cu (100) surfaces or sandwiched in bulk Cu. The important difference between both configurations is that impurity atoms have in the sandwich configuration double as many Cu nearest neighbors as in the overlayer, so that the hybridization between the monolayer and the Cu host is strongly increased. Nevertheless the moments of the Fe and Co monolayers are rather stable and are only slightly reduced. Only for Ni layers a larger effect is found. Whereas for the Ni overlayer a small local moment of 0.16 μ_B is found, the Ni moment is completely quenched for the sandwich configuration.

For the (100) monolayers embedded in Cu we have performed a detailed study of the host polarization in the neighboring monolayers. The results for the Cu hyperfine fields H_n are shown in fig. 6. Since the host polarization decreases asymptotically as $1/d_n^2$, where d_n is the distance between the monolayer and the nth neigh-

Table 4
Calculated local moments of (100) monolayers of Fe, Co and Ni as overlayer (OL) on the Cu substrate or as sandwich layer (SL) in bulk Cu (in units of μ_B).

	Fe	Co	Ni
OL	2.70	1.71	0.16
SL	2.50	1.55	≈ 0

boring Cu layer, we have plotted in fig. 6 the product $H_n n^2$, so that a pure oscillatory behavior remains for large distances. From the figure one sees that the oscillations for the Fe and Co layers are rather similar and more or less phase shifted for larger distances. The somewhat irregular behavior suggests that more than one period determine the oscillations, as one expects from the analysis of the asymptotic behavior [21].

In contrast to the similar behavior for larger distances, the hyperfine fields for the neighboring Cu layer are appreciably different. For instance, the hyperfine field of the neighboring Cu layer is −100 kG in the case of the Fe monolayer, but only −36 kG for the Co monolayer. The large differences can be estimated from the impurity results. For a Cu atom of the first neighboring layer the dominant contribution arizes from the four nearest neighbor impurity atoms, yielding about −143 kG for the Fe layer, but only −53 kG for the Co layer.

We will now shortly discuss calculations concerning magnetic monolayers sandwiched into bulk Pd. For the (100) Fe monolayer we obtain a local moment of 2.80 μ_B, being somewhat smaller than the 3.19 μ_B obtained for the (100) Fe overlayer on Pd (100) [22]. Similar for the Co overlayer we obtain a moment of 1.75 μ_B, compared to the moment of 2.12 μ_B for a Co overlayer on Pd (100) [22]. Naturally the reduction is due to the stronger hybridization with the d band of Pd.

The corresponding Pd polarization around an Fe monolayer is shown in fig. 7. For the first Pd layer we calculate induced moments of about 0.23 μ_B. These are considerably larger than the moments of about 0.1 μ_B induced on nearest neighbor Pd atoms in the impurity case. Basically the difference is due to the fact that in the monolayer geometry the neighboring Pd atoms have four impurity atoms as nearest neighbors, leading to larger induced moments. As can be seen from the semilogarithmic plot of fig. 7, the moments decrease essentially exponential for larger distances. Up to the seventh layer, no indication of oscillations are found. The total

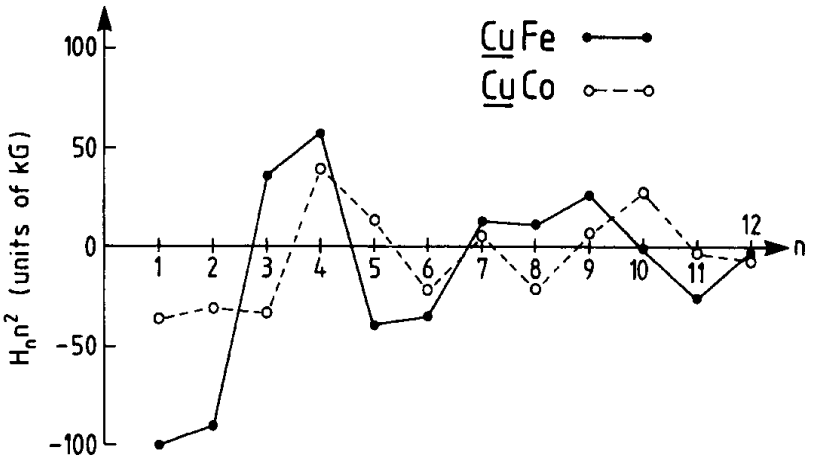

Fig. 6. Hyperfine fields H_n of Cu atoms in the nth layer around Fe and Co (100) monolayers in bulk Cu. Plotted are the hyperfine fields H_n times n^2.

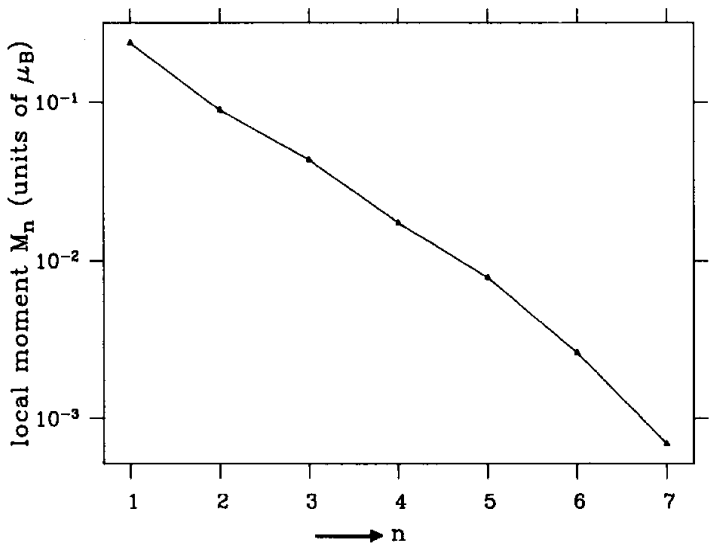

Fig. 7. Induced local Pd moment M_n on the nth host layer around an Fe(100) monolayer in Pd (semilogarithmic plot, units: μ_B).

induced Pd moment is about 0.8–0.9 μ_B for each Fe or Co impurity atom. These values are much smaller the corresponding values of 7–8 μ_B for Fe and Co impurities in Pd. Again the difference is a consequence of the different geometry. Each impurity can induce moments on twelve neighboring Pd atoms, which then induce moments on their neighbors etc., whereas for the monolayer geometry each impurity has effectively only two Pd neighbors to induce moments on.

Acknowledgement

We would like to thank M. Weinert for helpful discussion. We acknowledge support from North Atlantic Treaty Organisation Collaborative Research Grant No. 0086/88.

References

[1] S. Lundqvist and N.H. March, eds., *Theory of the Inhomogeneous Electron Gas* (Plenum Press, New York, 1983).
[2] P.J. Barspenning, R. Zeller, A. Lodder and P.H. Dederichs, Phys. Rev. B 29 (1984) 703.
[3] R. Zeller, P. Lang, B. Drittler and P.H. Dederichs, in: *Application of Multiple Scattering Theory to Materials Science*, MRS Symposium Proceeding, Vol. 253 (Materials Research Society, Pittsburgh, 1992) p. 357.
[4] D. Riegel, H.J. Barth, L. Büermann, H. Haas and Ch. Stenzel, Phys. Rev. Lett. 57 (1986) 388.
[5] D. Riegel, K.D. Gross and M. Luszik-Bhadra, Phys. Rev. Lett. 59 (1987) 1244.
[6] K.D. Gross and D. Riegel, Phys. Rev. Lett. 61 (1988) 1249.

[7] K.D. Gross, D. Riegel and R. Zeller, Phys. Rev. Lett. 63 (1989) 1176.
[8] B. Drittler, H. Ebert, R. Zeller and P.H. Dederichs, Phys. Rev. B 39 (1989) 6334.
[9] N. Papanikolaou, N. Stefanou, R. Zeller and P.H. Dederichs, Phys. Rev. B (1992).
[10] B. Coqlin and A. Blandin, Adv. Phys 17 (1968) 282.
[11] V.I. Anisimov and P.H. Dederichs, Solid State Commun. (1992).
[12] S. Blügel, H. Akai, R. Zeller and P.H. Dederichs, Phys. Rev. B 35 (1987) 3271.
[13] W.D. Brewer, in: *Low Temperature Nuclear Orientation*, eds. N.J. Stone and H. Postma (North-Holland, Amsterdam, 1986) p. 407.
[14] R. Zeller, *Modelling and Simulation in Materials Science and Engineering* (1992).
[15] L.M. Roth, H.J. Zeiger and T.A. Kaplan, Phys. Rev. 149 (1966) 519.
[16] J.F. Janak, Phys. Rev. 16 (1977) 255.
[17] H. Ebert, B. Drittler, R. Zeller and P.H. Dederichs, Phys. Rev. B 45 (1992) 1841.
[18] A. Oswald, R. Zeller and P.H. Dederichs, Phys. Rev. Lett. 56 (1986) 1419.
[19] C.L. Fu, A.J. Freeman and T. Oguchi, Phys. Rev. Lett. 54 (1985) 2700.
[20] R. Richter, J.G. Gay and J.R. Smith, Phys. Rev. Lett. 54 (1985) 2704.
[21] P. Bruno and C. Chappert, Phys. Rev. Lett. 67 (1991) 1602.
[22] S. Blügel, Europhys. Lett. 7 (1988) 743.

* * *

Presentation P.H. Dederichs

G. Schatz: Would there be significant change of the transferred magnetic hyperfine fields in Cu when you increase the thickness of Fe, which is sandwiched between the copper?

P.H. Dederichs: This is a difficult question. Presumably the hyperfine field of the first Cu layer would not change much, while the longer ranged oscillations might be phase shifted. This assumes, however, that the structure and the moments of Fe do not change much, which is presumably not the case for films of fcc Fe.

D.H. Chaplin: The fine structures seen in Fe for magnetic host are not reproduced in nearly the same resolution as in Ni. Do you comment on that?

P.H. Dederichs: Few years ago, we looked at NMR data around the impurities in Fe, but it looked to me that all these data, according to the literature, are not very reliable except the Mossbauer data where you can see the first and second shell only. But if you have some other information I believe it quite interesting.

H.-E. Mahnke: Iron in Cu, when it is in the small size and small fraction, has a fcc structure, whereas it changes to a bcc structure if it has sufficiently a large size. How do you handle this problem.

P.H. Dederichs: Of course there is a problem in fcc Fe, but when you have 1–3 monolayers I would not say it is a problem. However, if you really have bulk fcc Fe you will get all the well-known problem.

D. Riegel: You have calculated oscillations of the spin density in a ferromagnetic monolayer sandwiched by Cu layer. How do your calculated results for the oscillation period compare with the many experimental results of exchange coupling oscillations between magnetic layers sandwiched by nonmagnetic layers?

P.H. Dederichs: Up to now we have only calculated the host polarization due to a single monolayer, but not the interlayer coupling. We expect, however, this coupling to show very similar oscillations, since they are also determined by the host Green's function. The experimental observations of the coupling are strongly influenced by interface roughnesses, which tend to suppress the short range periods. At the present stage a direct comparison is not possible.

T.P. Das: Question: How practicable is it to include lattice relaxation effects by your procedure?

Comment: In the sixties and seventies for hyperfine properties of metallic systems our group was using primarily band-structure procedures. At the present time and over the past few years during, the eighties when we were working with impurity systems, we have been using Hartree–Fock cluster procedures (so far primarily for semiconductor hosts and ionic crystal hosts) which allow us to avoid the local density approximation and use real exchange and also include lattice relaxation effects more easily. It would be helpful to work on a few impurity systems by both your Green's function methods and the Hartree–Fock cluster procedure with correlation included if possible to both see how the results compare and the relative advantages and disadvantages of the two procedures. Thus, while you can work with essentially the infinite lattice because it includes bandstructure effects, the cluster procedures uses a finite lattice approximations. However, one always studies convergence with respect to cluster size and this procedure seems so far to be quite satisfactory for local properties like hyperfine structures.

P.H. Dederichs: Although it is somewhat more difficult as for other methods, lattice relaxations can be included into the KKR Green's function formalism and we have published some calculations along this line previously (N. Stefanou, P.J. Braspenning, R. Zeller and P.H. Dederichs, Phys. Rev. B 36 (1987) 6372). However, at present we are not able to calculate the relaxation self-consistently.

K. Krop: Is the Fe monolayer sandwiched between Cu ferromagnetic of antiferromagnetic? In other words, does the magnetic structure influence the results of your calculations?

P.H. Dederichs: The considered Fe monolayer is ferromagnetic. Ab initio calculations (S. Blügel, M. Weinert, P.H. Dederichs, Phys. Rev. Lett. 60 (1988) 1077) show that this structure is more stable than the in-plane c(2 × 2) antiferromagnetic structure. The host polarization would be very different for both structures.